Non-Invasive Real-Time Monitoring of Glucose Level Using Novel Microwave Biosensor Based on Triple-Pole CSRR

Ala Eldin Omer, *Graduate Student Member, IEEE*, George Shaker, *Senior Member, IEEE*, Safieddin Safavi-Naeini, *Life Fellow, IEEE*, Georges Alquié, Frédérique Deshours, Hamid Kokabi, *Member, IEEE*, and Raed M. Shubair, *Senior Member, IEEE*

***Abstract*—Planar microwave sensors are considered an attractive choice to noninvasively probe the dielectric attributes of biological tissues due to their low cost, simple fabrication, miniature scale, and minimum risk to human health. This paper develops and measures a novel microwave biosensor for non-invasive real-time monitoring of glucose level. The design comprises a rectangular plexiglass channel integrated on a triple-pole complementary split ring resonator (TP-CSRR). The proposed sensor operates in the centimeter-wave range 1–6 GHz and is manufactured using PCB on top of an FR4 dielectric substrate. The sensor elements are excited via a coupled microstrip transmission-line etched on the bottom side of the substrate. The integrated CSRR-based sensor is used as a near-field probe to non-invasively monitor the glucose level changes in the blood mimicking solutions of clinically relevant concentrations to Type-2 normal diabetes (70–120 mg/dL), by recording the frequency response of the harmonic reflection and transmission resonances. This indicates the sensor's capability of detecting small variations in the dielectric properties of the blood samples that are responsive to the electromagnetic fields. The proposed sensor is verified through practical measurements of the fabricated design. Experimental results obtained using a Vector Network Analyzer (VNA) demonstrate a sensitivity performance of about 6.2 dB/(mg/ml) for the developed triple-pole sensor that significantly outperforms the conventional single-pole and other proposed sensors in the literature in terms of the resonance amplitude resolution.**

Manuscript received July 1, 2020; revised September 18, 2020; accepted November 6, 2020. Date of publication November 17, 2020; date of current version December 30, 2020. This work was supported in part by the Natural Sciences and Engineering Research Council of Canada (NSERC), under Grant CREATE 509950-2018 Training in Global Biomedical Technology Research and Innovation, C-COM Satellite Systems Inc, Erasmus+ mobility grant, and in part by the Schlegel UW Research Institute of Aging (UW-RIA). *(Corresponding author: Ala Eldin Omer.)*

Ala Eldin Omer, George Shaker, and Safieddin Safavi-Naeini are with the Centre for Intelligent Antenna and Radio Systems (CIARS), Electrical and Computer Engineering, University of Waterloo, Waterloo, ON N2L 3G1, Canada (e-mail: aeomomer@uwaterloo.ca; gshaker@uwaterloo.ca; safavi@uwaterloo.ca).

Georges Alquié, Frédérique Deshours, and Hamid Kokabi are with the Group of electrical engineering Paris (GeePs), UMR CNRS-CentraleSupelec–University Paris-Saclay–Sorbonne University, 75252 Paris Cedex 05, France (e-mail: georges.alquie@upmc.fr; Frederique.deshours@sorbonne-universite.fr; hamid.kokabi@upmc.fr).

Raed M. Shubair is with the Department of Electrical Engineering and Computer Science, Massachusetts Institute of Technology (MIT), USA 02139, and also with the Department of Electrical and Computer Engineering, New York University Abu Dhabi, UAE 129188, Abu Dhabi (e-mail: rshuabir@mit.edu).

Color versions of one or more figures in this article are available at https://doi.org/10.1109/TBCAS.2020.3038589.

Digital Object Identifier 10.1109/TBCAS.2020.3038589

***Index Terms*—Complementary split-ring resonators, Debye model, dielectric characterization, microwave sensing, microstrip technology, non-invasive glucose detection.**

I. Introduction

DIABETES is a disastrous and growing problem, and its costs to the society are highly escalating. Over 450 million people worldwide suffer from diabetes and the number is increasing rapidly at an unpredictable rate according to the International Diabetes Federation (IDF) [1]. In North America, 37.0 million people have been with diabetes while in Canada about 5.0 million Canadians are expected to be with diabetes by 2025 according to the World Health Organization (WHO) [2]. Diabetes is described as a metabolic disorder of hormone insulin production by the pancreas, thus degenerating the cells' vitality in glucose absorption from the circulating blood. Therefore, diabetics' blood sugar is not naturally regulated within the normal range, thus needs an orderly inspection. By frequently monitoring the blood glucose, a diabetic patient would prematurely meet the desired glycemic target and hence avert being susceptible to critical complications such as heart disease, coma, stroke, kidney failure, and blindness [3]. Furthermore, avoiding undesired levels of hyperglycemia above 230 mg/dL and hypoglycemia below 65 mg/dL becomes possible if the glucose level is continuously monitored and appropriately adjusted, when needed [4]. This is also presented in the WHO 2016 report, indicating that regular diabetes monitoring via frequent BGL measurement is an essential preventive method to protect diabetic patients, beside the scaled-up prevention and enriched care [2].

The leading methodology used reliably by diabetics to check their glycemic level is the invasive self-monitoring blood glucose meters (Glucometers) that analyze the capillary blood samples drawn from the fingertips on a strip of test paper. These invasive devices could only provide BGL measurements at a specific time spot by the time of testing. Therefore, their readings will not reflect any long-term patterns or trends in glucose fluctuations due to specific lifestyles, diet regimes, or medication intakes. Apparently, the pain, expense, overthinking, and inconvenience associated with the current self-monitoring technology result into patient non-compliance for enduring adequate daily measurements, thus limiting the benefits of BGL self-monitoring.

1932-4545 © 2020 IEEE. Personal use is permitted, but republication/redistribution requires IEEE permission.
See https://www.ieee.org/publications/rights/index.html for more information.

Authorized licensed use limited to: Universitat de Barcelona. Downloaded on October 17,2024 at 13:45:49 UTC from IEEE Xplore. Restrictions apply.

TABLE I
MICROWAVE-BASED DIELECTRIC CHARACTERIZATION TECHNIQUES, THEIR PROS AND CONS

Technique	Examples	Pros	Cons
Free-Space Methods	MUT between two horn antennas connected to VNA (reflection/transmission based)	• Non-destructive (preserve the MUT integrity). • Contactless (easy sample preparation). • Wideband characterization.	• Need for large samples (large wavelength) to avoid diffraction on sample edges. • High cost for lenses and antenna equipment.
Transmission -Line Methods	MUT inside a transmission-line (e.g. waveguide or coaxial line) (reflection/transmission based)	• Cheaper (no need for lenses) • MUT characterized in the unimodal propagation band of the device • Wideband characterization. • Wider bandwidth at low frequencies (coaxial cables). • Simple MUT preparation (rectangular or circular inside waveguides). • Inexpensive	• Sample must be carefully prepared and adapted to the device shape (coaxial cables). • Narrow allowed bandwidth and characterization is valid for a limited frequency range (waveguides). • Less accurate (affected by asymmetries in sample surface). • Confined penetration depth. • Mathematical model complexity.
Near-Field Sensors	Open-ended coaxial lines (reflection based)		
Resonance Methods	• Ring resonator coupled to a transmission-line • Cavity resonator (Quality-factor and resonance frequency based)	• Reliable accuracy especially for MUT with low losses.	• Mainly for narrow band but harmonic resonances can be used for wideband characterization • Precise fabrication for resonator and sample preparation • Limited by the size and physical state of the sample

Therefore, a new demand for non-invasive pain-free blood glucose monitors is eminent to encourage more frequent glucose checks and thereby contribute more generously to diabetes care and prevention [5].

Significant research has investigated alternative non-invasive glucose detection (NGD) techniques over the last decade [6], including the optical methods where the glucose concentrations are identified using optical parameters like optical coherence tomography (OCT), Raman and fluorescence spectroscopy, and more [7], [8].

However, bulky and costly instruments are commonly required for such measurements at short wavelengths. The absorbance spectroscopy techniques, such as red/near-infrared and mid-infrared [9], use the scattering of light on biological tissue to detect optical signatures of glucose in blood. However, the expensive cost for implementation and the high sensitivity to changes in physiological and environmental parameters are generic deficiencies for these approaches. The enzyme-based electrochemical methods [10] have also been explored for sensing the glucose level obliquely by measuring the sweat and interstitial fluid (ISF) and correlate them to the glycemia in bloodstream. An improved sensitivity is scored, yet the lagging between the physical glucose changes in sweat, ISF, and blood remains a challenge. The RF/microwave sensing techniques [11]– [29] have shown to be more promising among the abovementioned methods due to the intact penetration of the electromagnetic (EM) waves into biological tissues unlike other ionizing radiation (e.g., X-rays) that might incur dicey effects. Such techniques are principally based on the theory of material characterization wherein the EM properties (i.e., dielectric permittivity and conductivity) of a person's blood are considerably affected by its glucose content, thus a promising correlation model is desired.

A variety of transmission and/or reflection techniques have been developed for material characterization (i.e., measuring the complex permittivity) in the microwave/RF region such as transmission-lines, free-space methods, resonant methods, etc. A method is chosen properly depending on the operating frequency, physical state (solid or liquid) of the material under test (MUT), its losses and volume. Out of the many RF/microwave characterization approaches, the resonance-based methods have earned a popularity for the different sensing applications (e.g., biomedical, industrial, safety, etc.) that require high degree of precision and sensitivity. Such resonant methods employ various types of microwave resonators suitable for characterizing the low-loss materials over a narrowband, however for wideband characterization, the harmonic resonances could be effectively used. Table I summarizes some of the most popular dielectric characterization and the pros and cons of each.

Many studies have focused on extracting the permittivity measurements for liquid samples of relatively high glucose concentrations in the low-frequency range using different setups based on the aforesaid techniques. For instance, the relative permittivity and conductivity for adults' blood samples were measured in the frequency range 0.5–20 GHz using an open-ended coaxial probe [11]. The study in [12] used resonant cavity structures in the frequency range 2–3 GHz for measuring glucose solutions in the range 0–3600 mg/dL. Different setups with antenna sensors were used in [13] and [14] for the frequency ranges 1.0–2.5 GHz and 5.0–8.5 GHz, respectively. U-shape antenna was utilized in [13] to track the 1000 - 4000 mg/dL glucose variations in aqueous solutions, while a patch antenna was tested in [14] for the 50–500 mg/dL glucose range. Open waveguide structures were used in [15] for frequencies up to 20 GHz where a 12^{o} phase difference was observed for a 500 mg/dL glucose change in aqueous solutions. Nevertheless, most of the aforesaid designs achieved a limited sensitivity that is inappropriate for ideal detection of glucose level. Additionally, quite complex and sophisticated technologies were used for fabricating the sensor device and its attached circuitry.

Sensing modules in the millimeter(mm)-wave range have also been explored to enable shorter wavelengths and relatively large

Authorized licensed use limited to: Universitat de Barcelona. Downloaded on October 17,2024 at 13:45:49 UTC from IEEE Xplore. Restrictions apply.

penetration depth sufficient to probe the glucose concentrations in thin bodily tissues. For instance, in another work [16] we proposed a novel sensing modality that utilized a 60 GHz Frequency Modulated Continuous Wave (FMCW) radar to monitor BGLs. The system was tested to identify different synthetic blood samples of clinically diabetes-relevant concentrations (50–350 mg/dL) through analyzing the backscattered signals from the sample-filled test tube placed at 1 cm distance from the radar sensor. The mm-wave spectrum has also been studied in [17] to design a pair of 60 GHz microstrip patch antennas and the $|S_{21}|$ magnitude was used to detect the varying-levels glucose samples loaded onto an acrylic tank installed between the two antennas. The system has shown a poor sensitivity of about 0.25 dB per 1000 mg/dL change in glucose concentrations.

Metamaterial-inspired microstrip-coupled resonators of small electrical size like split-ring resonator (SRR) and its complementary (CSRR) are more favored in sensing and characterization applications for their accuracy, miniature size, simple fabrication, easy integration, and high sensitivity [18]– [25]. Two SRRs were integrated in [22], one resonator was used for sensing the glucose sample and the other was set as a reference to revoke the temperature effects. Another metamaterial resonator operating at 3–5 GHz was proposed in [23] for detecting the 68–150 mg/dL concentrations in small droplets of human serums. A closed-loop SRR operating in 2–5 GHz was recently proposed in [24] to detect 50–400 mg/dL aqueous glucose concentrations on the $|S_{11}|$ reflection response at a sensitivity of about 82 MHz/(mg/ml). Three versions of an open-loop microstrip resonator operating between 2–7 GHz were analyzed in [25] for testing small volumes 5–25 μL of highly concentrated glucose aqueous solutions 1250–10000 mg/dL inside a dielectric liquid holder pasted onto their gaps. The Q-factor and maximum $|S_{21}|$ magnitudes were used as primary sensing parameters. However, reported measurements have shown very limited sensitivity inadequate for practical blood glucose monitoring in diabetes.

We find the resonant CSRR-based microwave sensing approach more attractive to develop a viable compact planar microwave biosensor for non-invasive glucose detection due to the following reasons:

- Sensing the complex permittivity of glucose tissues more efficiently using low power with a simple design and affordable fabrication process.
- Fully compliant to the green form of technology that features the non-invasive measurements in nondestructive fashion. Therefore, no hazards or risks to the human health when revised for continuous BGL monitoring in a wearable format.
- Unlike the SRRs, CSSRs are more reactive to MUT's permittivity changes due to the electric field spreading in a larger circumference beyond the narrow slits of SRRs.
- The electrical size of the sensor is relatively small which allows for a compact miniaturized realization.
- The coupled electric field is highly concentrated and localized in a relatively large sensing region, thus boosting for an improved sensitivity and imaging capability given the lossy nature of glucose samples.

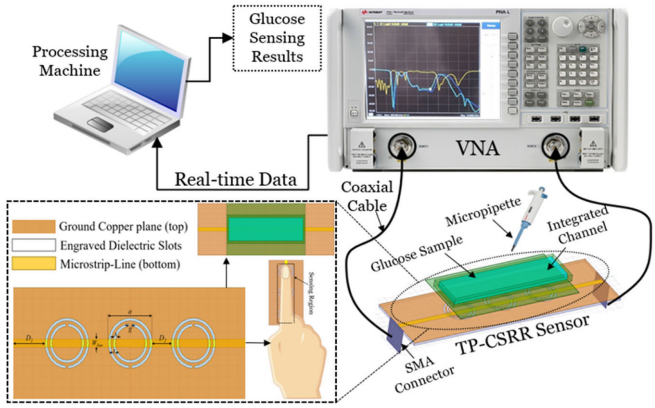

Fig. 1. Proposed TP-CSRR sensing system for blood glucose monitoring.

- The unlimited reusability and good accuracy throughout the sensor lifespan eliminate the need for any replacement as in the case of the implanted sensors, patches or devices that use chemical reactions or fluid transfer through the skin.

Therefore, and towards realizing a wearable non-invasive blood glucose monitor, we propose a highly sensitive miniaturized microwave biosensor working in the low centimeter-wave band (1–6 GHz) that favors sufficient penetration depth ($\sim$ 0.4–3 cm) and interaction of EM waves with the epidermis/dermis tissues of human body [26], [27], while allowing for sizing smaller sensing structure. It consists of three cells of complementary split-ring resonators (CSRRs) coupled to a planar microstrip-line etched on top of a thin dielectric substrate. A coaxial line is used to feed the microstrip-line from an RF power supply at the operating frequency. The integrated sensing system is shown in Fig. 1.

The primary objective of the proposed sensor is to monitor the change in blood glucose of small concentrations (70–120 mg/dL) clinically relevant to Type-2 diabetes. In this preliminary prototype, synthetic blood glucose tissues of desired concentrations are loaded at a precise volume on top of the sensor inside an integrated vein-like channel. The glucose-contained tissues–of high permittivity and dielectric loss characteristics–would consequently perturb the intrinsic electric field distribution in the sensing region over the CSRR cells. This would enable the CSRR sensor to identify various glucose levels via tracing the depth/amplitude and/or frequency variations of the reflection and transmission resonances at multiple frequencies. Different layouts of the TP-CSRR sensor are developed and studied using the 3D full-wave finite element simulator (ANSYS HFSS) where the different geometrical parameters of the sensor are numerically analyzed and optimized. A wearable model incorporating diabetes-related glucose concentrations on top of a skin tissue is also numerically simulated to study the sensitivity performance with respect to changes in blood permittivity that is glucose-level dependent. The functional behaviour of the TP-CSRR structure is electrically modelled using an optimized lumped-element equivalent circuit developed in ADS (Advanced Design System)

Authorized licensed use limited to: Universitat de Barcelona. Downloaded on October 17,2024 at 13:45:49 UTC from IEEE Xplore. Restrictions apply.

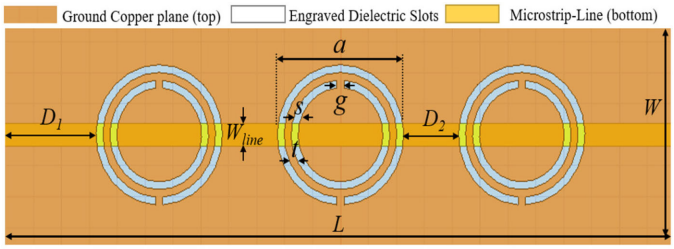

Fig. 2. Configuration of the CSRR poles in the ground plane (top view).

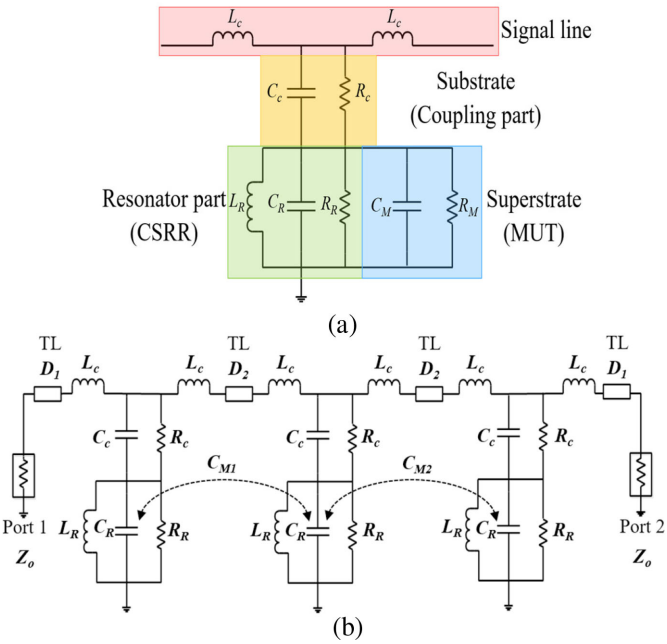

Fig. 3. Equivalent electrical model of (a) single CSRR cell under loading condition, (b) unloaded triple-pole CSRR.

software. The low-cost laser-incorporated PCB manufacturing is used to fabricate the sensor prototype on a thin dielectric sheet. The sensitivity performance of the fabricated prototype for detecting the glucose concentrations of interest is practically demonstrated by the in-lab measurements using a VNA setup.

The remaining sections of this paper are organized as follows: Section II explains the design perspectives and specifications, electrical modelling, numerical simulations, and fabrication processes of the proposed sensor. The numerical analysis of the sensor for glucose sensing is discussed in Section III. The in-lab measurements results and performance analysis are presented in Section IV. Section V concludes the paper and outlines the future work.

II. Proposed Microwave Glucose Biosensor and Glucose Sensing Principle

The proposed sensor design is primarily inspired from the very basic geometry of split-ring resonators with localized elements. The sensor structure is composed of three similar cells of complementary split-ring passive resonators (CSRRs) patterned horizontally on the top layer of a dielectric substrate of length L, width W, and thickness h. The first cell is located at distance D_1 from the input port. The CSRR cells are spatially detached with D_2 distance ranges from one cell boundary to another as depicted in Fig. 2. Each CSRR cell is composed of two concentric split-rings of dielectric slits nested inside each other and engraved in the copper ground plane. The double split-rings are designed in the form of two circular-shaped annular loops with a gap t between each as shown in Fig. 2. The loop of each ring ends in a metallic slot of width g. The three resonators are coupled with the RF power supply via a copper microstrip-line (MTL) of L_{line} length and W_{line} width as etched on the bottom face of the dielectric substrate.

This sensing structure induces charges and currents inside the engraved dielectric rings, yielding inductances and capacitances with stored oscillating energies (electric and magnetic). The microstrip sensor resonates at a specific frequency once both energies are balanced. In principle, the intrinsic resonance characteristics (resonant frequency, width, depth, and Q-factor) are all determined by the physical dimensions of the sensor geometry as well as the dielectric specifications of the base substrate [28]. The stored electric energy/field interacts with the surrounding medium or MUT (i.e., glucose sample) placed in close proximity of the CSRRs, and therefore, any permittivity mutations in the MUT can be related to the created effective capacitance of the resonant structure. Accordingly, the glucose sensing principle for this CSRR sensor is based on the capacitive perturbation caused by disturbing the electric field distribution in the presence of the glucose sample under test. This sample is applied on the CSRRs surface in a region where the electric field is highly concentrated to acquire the most interaction with the coupled fields at the resonant frequency. The resulting changes in resonance profile are considered as a signature of the sample dielectric properties that could be correlated to the corresponding glucose level through careful analysis of the modified resonance behaviour.

A. Electrical Modelling of TP-CSRR

Simple quasi-static models of lumped elements can be used to describe the physical behavior of the CSRRs given their smaller dimensions compared to the guided wavelength ($<\lambda_g/10$) [30]. To electrically model the TP-CSRR, a model common to different forms of resonators is developed for each pole (SP-CSRR) based on localized *RLC* elements in the equivalent electrical circuit shown in Fig. 3(a). An inductance L_c is used to model the magnetic coupling of the MTL strip when crossing the CSRR cell for excitation. A shunt capacitance C_c models the dielectric substrate that guides the EM fields from the MTL to couple the resonator in the ground plane. The losses of both substrate and metal ribbon are represented by R_c. An *RLC* parallel resonant circuit is used to describe the behaviour of the resonator part. Particularly, L_R depicts the windings of width s in the interior/exterior rings, C_R captures the capacitances created in the metallic gaps g and spacings t, and lastly R_R models the conductive and dielectric losses including the small magnetic losses associated with L_R.

Given this structure, the resonant frequency of the single cell is given by $f_o = \frac{1}{2\pi\sqrt{L_R(C_R + C_c)}}$ and its unloaded Q-factor is

Authorized licensed use limited to: Universitat de Barcelona. Downloaded on October 17,2024 at 13:45:49 UTC from IEEE Xplore. Restrictions apply.

TABLE II
CHARACTERISTIC FREQUENCIES AND CALCULATED REACTIVE ELEMENTS OF THE SP-CSRR ELECTRICAL MODEL

f_o (GHz)	f_S (GHz)	f_R (GHz)	f_Z (GHz)	f_C (GHz)	L_R (nH)	C_R (pF)	L_C (nH)	C_C (pF)
2.30	1.62	3.04	1.93	3.55	2.16	1.27	2.12	0.95

$Q = \frac{f_0}{\Delta f_{3\text{dB}}} = 2\pi f_o R_P (C_R + C_c)$, where $\Delta f_{3\text{dB}}$ represents the 3 dB bandwidth of the resonance peak, and R_p is the equivalent resistance of paralleling the coupling-part R_c and resonator-part R_R. When a sample (superstrate) is loaded onto the resonator, an *RC* parallel circuit is attached to the resonator part to model the EM properties (ϵ'_r and $tan\delta$) of the loaded sample. To elaborate, C_M is directly related to the relative permittivity of the sample while its loss property is linked to R_M. In consequence, changes in the dielectric characteristics of the loaded MUT (i.e., glucose) are reflected into f_o and Q through perturbing the CSRR effective capacitance and resistance. Therefore, when the integrated CSRR sensor is used for sensing a given glucose sample, all the model parameters would be fixed in value except for the resonator part that is essentially controlled by the EM properties of the glucose sample. The model for SP-CSRR can be extended to TP-CSRR by modelling the in-between line-delays between individual poles using the transmission-line model as shown in Fig. 3(b). Mutual coupling would take place between adjacent poles as represented by C_{M1} and C_{M2} capacitances.

The delay of each MTL segment was estimated using the relation $T_D = \frac{\epsilon_{eff}}{\omega}$, where ϵ_{eff} is the effective permittivity of the MTL evaluated at the operating frequency ω based on the substrate specifications as well as the thickness, width and length of the MTL segment. For illustration, to electrically model the line-delay of $D_2 = 3.92$ mm between adjacent cells, the Line-Calc module in ADS was used to calculate the corresponding ϵ_{eff} and Z_o at $\omega = 2.3$ GHz given the substrate specifications ($h = 0.8$ mm, $\epsilon'_r = 4.4$, and $tan\delta = 0.02$) as well as the thickness, width and length of the TL ribbon segment ($W_{seg} = 1.5$ mm, $t_{seg} = 35$ μmm and $L_{seg} = 3.92$ mm) resulting into $\epsilon_{eff} = 0.34$ rad, $Z_o = 50.31$ Ω, and a delay value of 24.17 ps. The reactive elements (C_C, L_C, C_R, L_R) of the TP-CSRR model were initially calculated by solving the system of equations in [31] for the four characteristic frequencies (f_s, f_o, f_R, and f_z) observed in the frequency responses (S_{11}, S_{21}, and Z_{11}) of the de-embedded SP-CSRR. Particularly, f_s and f_o are the minimum resonance frequencies of the reflection $|S_{11}|$ and transmission $|S_{21}|$ coefficients, respectively. f_R and f_z are observed in the input impedance Z_{11} response as calculated from the measured S-parameters in the open circuit mode of the SP resonator. Z_{11} has a minimum value at frequency f_z and a very high value at frequency f_R that represents the resonance frequency of the parallel circuit equivalent to the resonator only. The values for both sets are documented in Table II.

The lumped elements model was then implemented in ADS using the exact values in Table II, and further optimized to match the S-parameter measurements collected via VNA for the unloaded SP-CSRR. The dielectric losses (resistive elements R_R and R_c) were first estimated by considering the loss tangent of the FR4 substrate and the value of the corresponding capacity, then optimized from the amplitudes and widths of the reflection and transmission resonances. Figures 4(a) and 4(b), compare the results of simulating the electric schema of SP-CSRR before and after optimizing its respective elements in ADS to those experimentally measured when unloaded. The calculated and optimized values for the resistive and reactive elements of the electrical circuit are presented in Table III. The differences between the estimated and optimized values remain in a reasonable range, thus validating the proposed electrical model and methodology. The analytical values of the exclusive SP-CSRR part are integrated into the TP-CSRR model of Fig. 3(b) and further fine-tuned to match the experimental TP-CSRR measurements of reflection and transmission coefficients as shown in Fig. 5(a) and 5(b), respectively. The optimized values of the lumped elements are shown in Table IV.

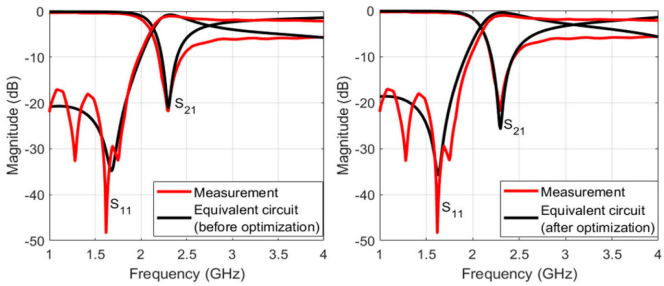

Fig. 4. S-parameters from VNA measurements and ADS electrical simulation for the SP-CSRR model, (a) before optimization and (b) after optimization.

TABLE III
ANALYTICAL VALUES OF THE LUMPED ELEMENTS MODEL OF THE SP-CSRR

Parameter	L_R (nH)	C_R (pF)	L_C (nH)	C_C (pF)	R_C (kΩ)	R_R (kΩ)
Calculated	2.16	1.27	2.12	0.95	4.4	3.0
Optimized	1.78	1.55	2.71	1.15	4.99	3.29

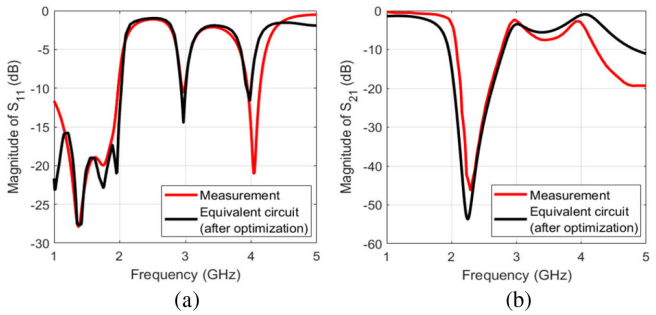

Fig. 5. S-parameters from VNA measurements and ADS electrical simulation for the TP-CSRR optimized model, (a) reflection and (b) transmission coefficients.

Authorized licensed use limited to: Universitat de Barcelona. Downloaded on October 17,2024 at 13:45:49 UTC from IEEE Xplore. Restrictions apply.

TABLE IV
OPTIMIZED VALUES OF THE TP-CSRR LUMPED ELEMENTS MODEL

L_R (nH)	C_R (pF)	L_C (nH)	C_C (pF)	R_C (kΩ)	R_R (kΩ)
3.33	0.63	3.38	0.88	1.30	1.32

B. Design Perspectives

The EM dispersive properties of blood tissues (ϵ'_r and $tan\delta$) change very slightly for varying-level glucose spectrum of diabetics (60–300 mg/dL). For instance, the single-pole Debye model in [32] suggests that for a 20 mg/dL glucose change at 2.3 GHz, the percent change in $tan\delta$ is about 0.8% while that in ϵ'_r is around 0.01%. Therefore, for blood glucose monitoring applications, we need to optimize the design of the proposed sensing structure in terms of the geometric parameters defining the planar MTL and the CSRR resonating cells; in order to maximize the resonance strength and perfectly confine the resonating electric fields within the permittivity sensing region. This is pivotal to acquire higher sensitivity capable of capturing the small contrast in blood glucose dielectric properties. In what follows, the choice of integrating three cells and other design specifications are explored following thorough investigation of the sensitivity performance at different number of CSRR cells, resonator order (i.e., single or double loop), excitation schemes, substrate thickness, and CSRR geometries. The HFSS numerical simulator based on Finite Element Method (FEM) is used in these numerical analysis and modelling.

1) CSRR Orientation or Excitation Method: The integrated CSRRs could be either electrically excited when their magnetic walls (line of symmetry) are orthogonal to the coupling MTL, or possibly triggered by a combined electric/magnetic excitation when the magnetic walls are in parallel alignment with the MTL strip. Numerical analysis revealed a better sensitivity performance for the sensor when the CSRRs are oriented perpendicularly to the MTL strip. This would guarantee an electric excitation for the resonance with time-varying electric field between the MTL and the ground plane.

2) Substrate Thickness & Dielectric Properties: In the sensor structure of MTL coupled with the CSRRs, the plugged electric field polarizes a portion of the dielectric substrate and a portion of the loaded glucose sample. The sensor sensitivity to variations in glucose levels could be enhanced by increasing the dependency of the minimum transmission resonant frequency on the loaded sample permittivity (i.e., C_M). This is achieved by increasing the polarized portion of the loaded sample and decreasing the field confinement into the substrate by reducing its respective thickness h and dielectric properties (ϵ'_r and $tan\delta$). Lower substrate thickness of $h = 0.8$ *mm* has achieved better sensitivity compared to 1.6 mm thickness.

3) CSRR Cell Geometry: In addition to the substrate specifications, the resonant characteristics of the TP-CSRR sensor (f_o and Q) are also dependent on the geometrical parameters of each CSRR cell (diameters of both inner and outer rings a, coupling gap t, ring width s, and split gap g). HFSS was used to investigate the primary influence of each of these parameters on f_o. The pole diameters a and b are proportionate to the effective length

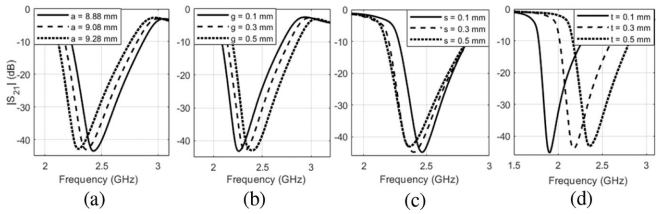

Fig. 6. Simulated transmission coefficients of unloaded TP-CSRR at different (a) outer diameter a (b) split-gap g (c) ring-width s (d) slots-coupling distance t

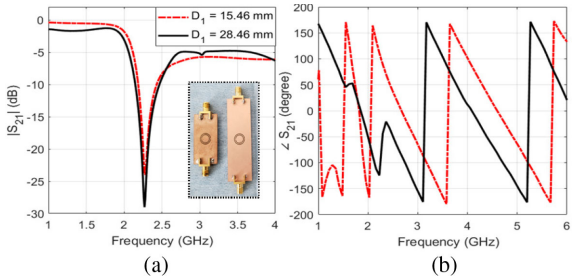

Fig. 7. Measured (a) transmission coefficient, and (b) transmission phase of the short and long SP-CSRRs.

of the dielectric slits; larger inductance L_R would be resulted for increased pole diameters, thus reducing the overall f_o as shown in Fig. 6(a) for the case of a changing from 8.88 to 9.28 mm. Fig. 6(b) depicts how f_o is shifted upward when increasing the split-gap g (reducing C_R) from 0.1 to 0.5 mm. Similar behavior with larger shifts in f_o is observed in Fig. 6(d) for increasing the slits-coupling distance t in 0.1, 0.3, and 0.5 mm. Fig. 6(c) also shows the slight decrease in f_o with an increased ring width s that is directly proportional to L_R. On the contrast, both slots-coupling distance t and split-gap g tend to establish an inverse proportionality to C_R, therefore increasing these parameters would probably increase f_o. The cells geometry has been optimized to reduce the combined reactive elements L_R and C_R in each cell and increase the minimum transmission frequency f_o towards 2.3 GHz, so that to realize more dependence on the loaded MUT permittivity (i.e., C_M).

4) Input Line-Delay D_1: The effect of the input delay D_1 (distance from the feeding port to the cell boundary) on the resonance profile was investigated numerically and experimentally to set it accordingly in the TP-CSRR design for utmost sensitivity. Two SP-CSRRs with different input delays $D_1 =$ 15.46 mm and $D_1 = 28.46$ mm were compared, when unloaded, in terms of the transmission coefficients and phases as functions of frequency as plotted in Fig. 7. Increasing D_1 enables the exciting signal to have sufficient propagation within and around the spatial extent of the MTL before coupling the resonator. Noticeably, D_1 does not have any effect on the transmission resonance frequency, which is shown in Fig. 7(a) to be around 2.295 GHz for both types. However, D_1 has an obvious effect on the resonance peak in the transmission mode where a 5 dB difference is recorded between the long (solid black) and short (dash-dotted red) SP-CSRRs. The effect of D_1 is more apparent

Authorized licensed use limited to: Universitat de Barcelona. Downloaded on October 17,2024 at 13:45:49 UTC from IEEE Xplore. Restrictions apply.

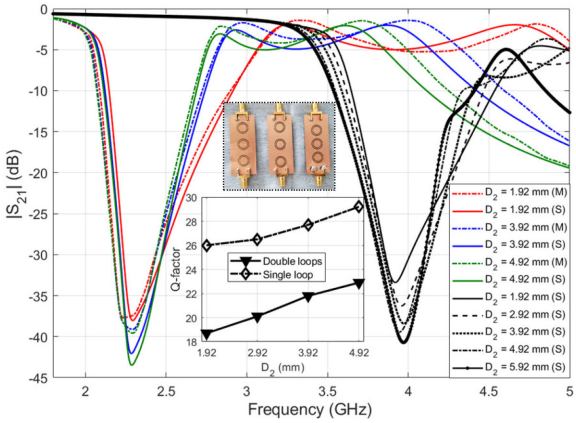

Fig. 8. Measured (M) and simulated (S) transmission coefficients of single and double-loop TP-CSRRs with different in-between line-delay D_2.

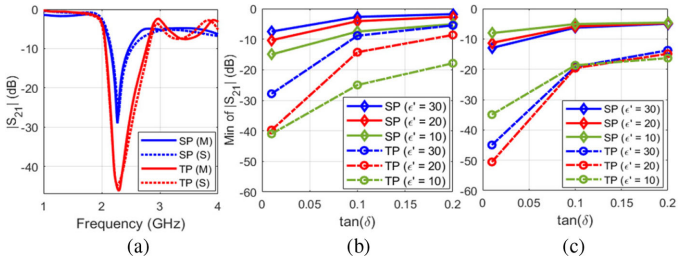

Fig. 9. (a) Measured and simulated transmission coefficients of the SP-CSRR and TP-CSRR sensors prior loading (resonance around 2.3 GHz). Comparing the behavior of SP-CSRR and TP-CSRR for changes in dielectric properties of a loaded sample at (b) fundamental resonance, and (c) harmonic resonance.

in the transmission phase response that tends to shift toward lower frequencies for larger D_1 as shown in Fig. 7(b).

5) In-Between Line-Delay D_2: Similarly, to examine how the resonance profile of the TP-CSRR is correlated to the delay parameter D_2 that represents edge-to-edge distance between adjacent poles, three TP-CSRRs with different delays D_2: 1.92, 3.92, and 4.92 mm, were numerically analyzed by comparing their transmission coefficients in the unloading state as shown in Fig. 8.

Apparently, D_2 would not affect the frequency of the minimum transmission response. However, increasing D_2 to some extent results into deeper resonance amplitude/depth, narrower 3- dB bandwidth, and a higher Q-factor for the TP-CSRR, thus benefiting a higher sensitivity for glucose detection as we will see later in Section III. This behavior is attributed to the inter-resonator coupling established between the adjacent poles. Similar behaviour was also demonstrated for the single-loop version that resonates around 3.9 GHz as shown in Fig. 8. It is also observed that TP-CSRR of single-loop excels the double-loop type in terms of the Q-factor as depicted in the enclosed graph (details about this sensitivity performance comparison are beyond the scope of this study).

6) Number of CSRR Cells: The CSRR cells are basically coupled to the MTL quasi-TEM mode of high intensity within confined area of the attached dielectric substrate. This will restrict any ground defect design for the CSRR to be positioned in small region within the hosting MTL for proper excitation. To overcome this limitation and realize a larger sensing region of concentrated electric field, we chose to integrate three cells of CSRR while exploiting the mutual coupling originated between each. In this section, the performance of the TP-CSRR sensor is analyzed both experimentally and numerically and compared to that of the conventional SP-CSRR. First, before loading any glucose sample, the transmission coefficients $|S_{21}|$ for both SP-CSRR and TP-CSRR were measured and simulated as plotted in Fig. 9(a). Both sensors exhibit initial resonances around $f_o = 2.3$ GHz. However, TP-CSRR is shown to have a steeper resonance peak/depth of around -46 dB amplitude compared to -24 dB for the case of SP-CSRR. In addition, the 3- dB bandwidth is more broadening in the TP-CSRR resonance than its corresponding on SP-CSRR. Results of Fig. 9(a) also verify our design with the good agreement between numerical simulations and practical measurements of the proposed sensor.

Second, both sensors were numerically analyzed to study the variation of their transmission responses to changes in dielectric constant and loss tangent of a loaded sample of a rectangular shape (36×20 mm^2). The S_{21} has been chosen for monitoring this variation since it shows the effect of the sample permittivity more predominantly, compared to S_{11}. The parametric sweep function in HFSS was used to vary the ϵ_r' between 10, 20, and 30, while for each value the loss tangent, *tanδ*, changes between 0.01, 0.1, and 0.2. Interestingly, upon loading such dielectric samples on top of each sensor, higher order harmonic resonances start to appear above 3 GHz. It is observed that increasing ϵ_r' causes a reduction in the transmission resonance frequencies. The sensors also exhibit variations in the resonance peaks to reflect the changes in *tanδ* of the loaded sample. This is evidenced by the gradual decline in the magnitude of S_{21} as the loss tangent increases from 0.01 to 0.2 as shown in Figs. 9(b) and 9(c) for the fundamental and harmonic resonances, respectively. In addition, it is observed that for a high lossy sample, 0.2 for example, both fundamental and harmonic resonances encountered very small dips in the SP-CSRR. However, this depth becomes larger when the lossy sample is tested on top of TP-CSRR.

The sensor with three CSRRs exhibits higher sensitivity with a steeper resonance peak/depth of around -46 dB amplitude at $f = 2.3$ GHz compared to -35 dB and -24 dB for the case of the DP-CSRR (double-pole) and SP-CSRR (single-pole), respectively. Therefore, TP-CSRR would probably yield a better sensitivity for characterizing lossy materials of high *tanδ*, which makes it ideal for adoption in our case to detect tiny variations in the loss tangent for various blood glucose concentrations of interest. Additionally, having three cells coupled together in the proposed sensor would allow for sensing the glucose-contained tissue over a larger region of the CSRRs, where the electric field is localized with high concentration, thereby acquiring higher sensitivity for glucose monitoring. Lastly, the effective area of about 37×9 mm^2 for the respective sensing region (with three cells) is quite adequate to place the subject finger when the sensor is adapted for non-invasive BGL monitoring as a wearable device.

Authorized licensed use limited to: Universitat de Barcelona. Downloaded on October 17,2024 at 13:45:49 UTC from IEEE Xplore. Restrictions apply.

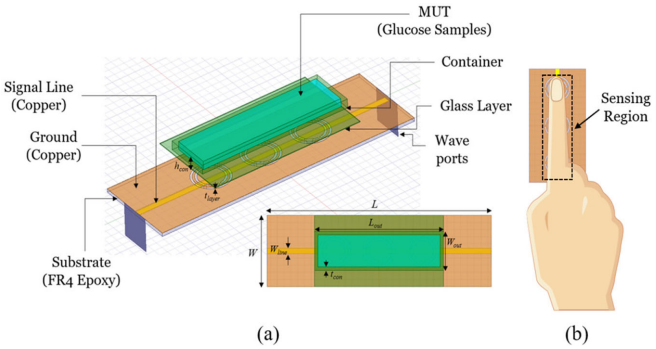

Fig. 10. (a) Geometrical schematic model of the TP-CSRR integrated with the vein-resembling channel (top view of the integrated sensor is enclosed), (b) sensor application for continuous glucose monitoring from the finger.

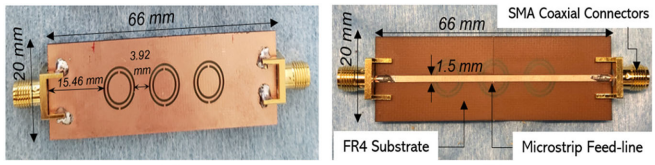

Fig. 11. Fabricated sensor prototype (a) top view showing the ground plane where the CSRR sensing elements were patterned, (b) bottom view showing the MTL used to excite the CSRRs.

TABLE V
EXTRACTED DIELECTRIC PROPERTIES FOR G1–G8 CONCENTRATIONS

Glucose samples	G_1	G_2	G_3	G_4	G_5	G_6	G_7	G_8
ϵ_r'	79.13	79.15	79.17	79.19	79.21	79.25	79.29	79.33
$tan\delta$	0.133	0.131	0.129	0.127	0.125	0.121	0.117	0.113

C. Proposed Sensor Design and Specification

Following the above-mentioned investigative studies, we used the FEM-based HFSS to design the proposed CSRR sensor in the triple-pole configuration depicted in Fig. 2. Specifically, three CSRRs were patterned on the upper face of an FR4 dielectric substrate ($\epsilon_r' = 4.4$ and $tan\delta = 0.02$) of length $L = 66$ mm, width $W = 20$ mm, and thickness $h = 0.8$ mm. The exterior ring of each CSRR cell was designed with outer diameter $a = 9.08$ mm, ring width $s = 0.5$ mm, and split gap $g = 0.5$ mm. Similar values were used for s and g in the interior ring of 8.08 mm outer diameter. The inter-distance t that considerably controls the coupling between the exterior and interior rings was optimized to 0.5 mm. The distances D_1 and D_2 were set to 15.46 mm and 3.92, respectively. The MTL was sized with a length of $L_{line} = 66$ mm and a width of $W_{line} = 1.5$ mm in order to realize a characteristic impedance of 50 Ω around 2.3 GHz that matches the internal input impedance of the feeding ports. A rectangular plexiglass container ($\epsilon_r' = 3.9$ and $tan\delta = 0.001$) was integrated on top of the CSRRs surface to hold the blood glucose samples. This would also simulate the practical scenario of the blood flow inside the blood vessels. The container has an outer length $L_{out} = 37$ mm, inner length $L_{in} = 36$ mm, outer width $W_{out} = 10$ mm, inner width $W_{in} = 9$ mm, wall thickness $t_{con} = 0.5$ mm, and height $h_{con} = 2$ mm. Additionally, a glass layer of slim thickness $t_{layer} = 0.15$ mm was introduced between the channel and CSRRs in order to evade short-circuiting the dielectric slots in each pole. Therefore, the damping effect on the reflection/transmission resonances can be significantly reduced when lossy glucose samples of moist nature are loaded on top. As a result, the resonance peaks remain indicative for the perturbation introduced when the blood glucose samples are loaded. Fig. 10(a) shows the final layout integrating the plexiglass rectangular channel with the CSRRs sensor. Illustration of the finger placement along the sensing region for continuous BGL monitoring is shown in Fig. 10(b).

D. Fabrication of the Sensor Prototype

A prototype of the TP-CSRR sensor was fabricated on an FR4 dielectric PCB of 35 μm copper layers on both sides using the laser micromachining (LPKF ProtoLaser U4). In this process, the scanning laser beam was initially used to etch three small holes as fiducials on the ground layer through the PCB to properly align top and bottom parts in the design. Next, the dielectric slots in the exterior and interior rings of each pole were engraved on the ground layer using the laser cutting. Lastly, the laser beam was used to pattern the MTL strip of 66 × 1.5 mm^2 cross section in the bottom later after alignment with the fiducials. A pair of 50 Ω SMA coaxial connectors were soldered to both ends of the MTL to facilitate the measurements when connecting to VNA. Fig. 11 shows both sides of the fabricated TP-CSRR prototype.

III. NUMERICAL ANALYSIS FOR GLUCOSE SENSING

In this section, the performance of the developed TP-CSRR sensor is numerically analyzed for non-invasive blood glucose detection. Aqueous glucose solutions were used in this analysis and later in the preliminary experiments to imitate the blood behavior at different glucose concentrations of clinically relevant to Type-2 diabetes, and to secure the repeatability of collected scattering measurements [33]– [34]. This is a rational approximation since water constitutes about 50% of the entire human blood where other components are present at varying proportions (e.g., sodium, calcium, chloride, potassium, etc.) [35]. These mineral constituents have lower concentrations, thus bring small effect onto the dielectric behaviour of blood compared to the dominant glucose that varies in a broad range as shown by Erdem *et al.* [36]. Aqueous-glucose samples of concentrations in the range 60–300 mg/dL were simulated on top of the sensing region inside the plexiglass channel as depicted in Fig. 10(a). This was done via integrating their respective dielectric properties over the operating frequency of the TP-CSRR in the HFSS simulator. Specifically, the Debye model proposed in [32] was used to approximate the dielectric permittivity and loss tangent parameters for the glucose concentrations of interest at $f =$ 2.3 GHz as listed in Table V. This model was developed in [32] for the permittivity dependency in glucose concentrations by fitting the dielectric measurements - collected using a commercial coaxial probe kit connected to VNA - of watery solutions of 50, 250, 1000, and 2000 mg/dL to a first order Debye relaxation model with the parameters shown in Table VI. According to this

Authorized licensed use limited to: Universitat de Barcelona. Downloaded on October 17,2024 at 13:45:49 UTC from IEEE Xplore. Restrictions apply.

TABLE VI
DEBYE COEFFICIENTS AS FUNCTIONS OF GLUCOSE CONCENTRATION [31]

Debye Parameter	Model
$\epsilon_\infty(\xi)$	$5.38 + (30 \times 10^{-3}).\xi$
$\epsilon_s(\xi)$	$80.68 - (0.207 \times 10^{-3}).\xi$
$\tau(\xi)$	$9.68 + (0.23 \times 10^{-3}).\xi$

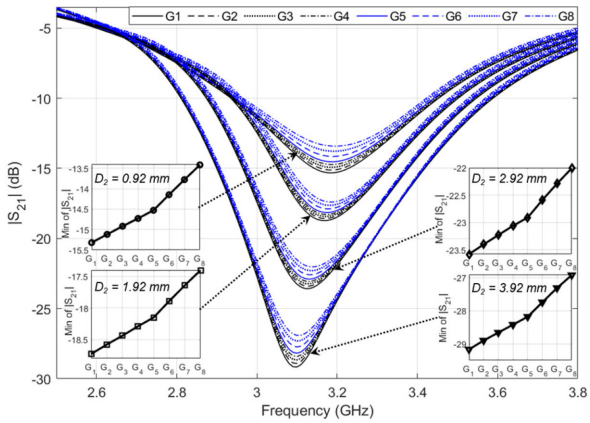

Fig. 12. Simulated transmission response of the TP-CSRR loaded with glucose concentrations at different D_2 models.

model, the relative complex permittivity for glucose aqueous solutions is defined as a function of the angular frequency $\omega = 2\pi f$ (rad/s) and the concentration ξ (mg/dL) of the dissolved glucose as given in (1) that uses the concentration-dependent Debye coefficients ϵ_{stat} (static permittivity), ϵ_∞ (infinity permittivity), and τ (relaxation time) [33]. The last term that uses the static conductivity σ_s and permittivity of free-space ϵ_o can be neglected for low-conductive materials.

$$\epsilon_r\ (w, \xi) = \epsilon_\infty\ (\xi) + \left(\frac{\epsilon_{stat}\,(\xi)\ -\ \epsilon_\infty\,(\xi)}{1\ +\ j\omega\tau\,(\xi)}\right) + \frac{\sigma_s}{j\omega\epsilon_o} \quad (1)$$

Fig. 12 shows the simulated transmission responses for the different samples G1–G8 loaded at volume 600 μL each. These responses were compared at different models of the in-between line-delay D_2 for the sensor to demonstrate the superiority of the proposed design at $D_2 = 3.92$mm as inferred from the higher amplitude resolutions $\frac{\Delta|S_{21}|}{\Delta|\epsilon_r'|} = 13.5$ dB and $\frac{\Delta|S_{21}|}{\Delta|tan\delta|} = 135$ dB compared to those of other models at $D_2 = 0.92$, 1.92, and 2.92 mm. The enclosed graphs show these resonant amplitude (min of $|S_{21}|$) variations at different glucose levels. To mimic the realistic scenario of placing a finger along the sensing region or when the sensor is revised as a wearable, we performed another simulation model where the glucose samples G1–G8 of thickness 2 mm each are placed on top of a skin layer ($\epsilon_r{}' = 38.1$ and $tan\delta = 0.28$) [22] of thickness 1 mm as depicted in Fig. 13(a). The electric field distribution induced by the coupled CSRR cells at resonance is plotted across the sensing region at two levels, $z = 0$ at the interface between the CSRRs surface and skin layer (Fig. 13(b)), and $z = 2$ mm inside the glucose tissue

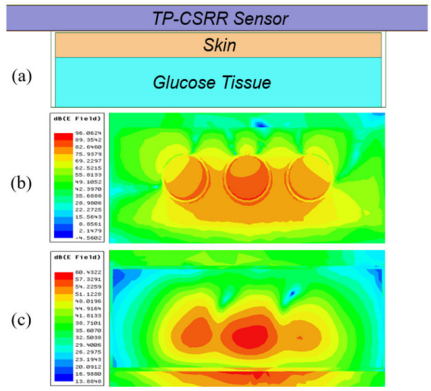

Fig. 13. (a) Cross section of the simulation model of the TP-CSRR loaded with glucose tissues on top of a skin layer. Electric field distribution across the sensing region at the interface between (b) TP-CSRR and skin, (c) skin and glucose tissue.

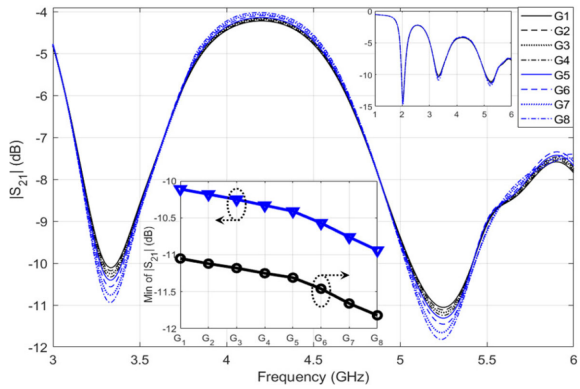

Fig. 14. Simulated transmission response of TP-CSRR loaded with different glucose concentrations on top of a skin layer.

(Fig. 13(c)). The sensor response was recorded over the range 3–6 GHz as depicted in Fig. 14, where two resonances were induced at $f = 3.3$ GHz and $f = 5.2$ GHz. The corresponding amplitude resolutions for glucose level changes were enclosed in Fig. 14.

IV. MEASUREMENT RESULTS AND PERFORMANCE ANALYSIS FOR GLUCOSE SENSING

A. Experimental Glucose Sensing Approach

The fabricated TP-CSRR prototype was practically experimented for detecting the glucose levels in two different tissues, aqueous solutions and synthetic blood (Hemoglobin-based). To mimic the practical condition of Type-2 diabetes, the tissues were precisely prepared in small disparate glucose concentrations 80, 100, and 120 mg/dL at 10 mL volume each using a micropipette device in the laboratory. To do so, volume V_1 was drawn from the stock glucose solution of $C_1 = 1000$ mg/dL as calculated using the dilution equation $C_1V_1 = C_2V_2$ to synthesize glucose aqueous samples of volume $V_2 = 10$ mL each at the desired concentrations $C_2 = 80$, 100, and 120 mg/dL. Another set of hemoglobin-mixed samples were prepared at the

Authorized licensed use limited to: Universitat de Barcelona. Downloaded on October 17,2024 at 13:45:49 UTC from IEEE Xplore. Restrictions apply.

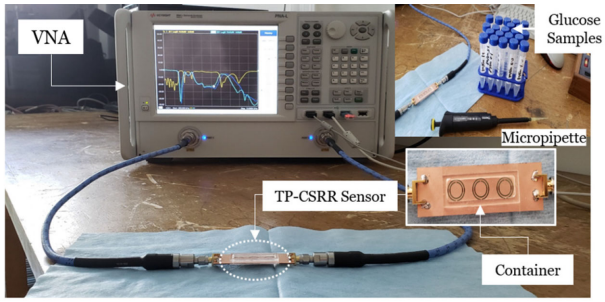

Fig. 15. Experimental setup for glucose sensing.

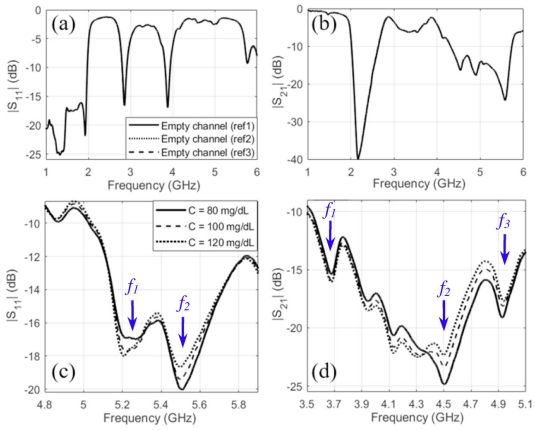

Fig. 16. Measured (a) reflection and (b) transmission coefficients over a broad band 1–6 GHz for the empty channel-loaded sensor. Measured (c) reflection and (d) transmission coefficients for the tested glucose samples on the higher frequency regions.

desired concentrations C_2 following the same recipe by adding volume V_1 from the standard glucose solution to V_2–V_1 of a pure fake blood instead of distilled water [37].

Measurements of the scattering responses from the sensor were performed using the Keysight Technologies PNA N5227A Network Analyzer by sweeping the frequency across the cm-band 1–6 GHz. Before connecting the sensor with the VNA, its full two-port calibration was performed using the standard Open-Short-Load technique to eliminate any undesired effects on the measurements, and hence accurate producible measurements would be achieved. The S-parameters data were recorded at 25 °C room temperature, 1600 frequency points resolution, 50 Hz IF BW, and −10 dB input power for the testing port. The channel-loaded TP-CSRR was connected via coaxial cables to the VNA power source as shown in the complete experimental setup in Fig. 15. First, before loading any glucose sample, the reflection and transmission responses of the TP-CSRR were measured and verified as plotted in Fig. 16(a), and 16(b), respectively. Next, the TP-CSRR sensor was tested for detecting the glucose level in the three prepared aquatic glucose samples of 80, 100, and 120 mg/dL. In each trial of the subsequent measurements, the micropipette device was used to measure a precise volume of $V = 600$ μL from a given concentration sample and load it inside the channel in three consecutive batches of 200 μL each. After each drop of $V = 200$ μL, noticeable shifts in the reflection S_{11} and transmission S_{21} resonances were observed towards lower frequencies which imply a dependency of the resonance frequency on the sample volume. However, these resonances were perfectly converged to a lower limit beyond the sample volume of 600 μL which enabled a homogenous distribution of the glucose sample inside the channel whereby the sensing area was entirely covered.

Based on the last result, the stable volume of 600 μL was adopted as a constant volume for testing all the glucose samples in the subsequent measurements to minimize the measurement errors due to uncertainty in the sample volume. Once a sample of given concentration was fully loaded then the corresponding reflection and transmission signals were recorded in the frequency band 1–6 GHz. The transmission response of the TP-CSRR loaded with an empty channel was considered as a reference for all measurements of glucose samples (Fig. 16(b)). A clean tissue paper was used after each measurement trial to completely remove the glucose sample in place before loading another concentration. This is important to reset the reference resonance at S21 prior-loading a new sample and hence guarantee precise measurements for fair comparisons.

The S-parameters corresponding to various tested glucose samples 80, 100, and 120 mg/dL were measured to record the resonance frequencies as well as their minimal amplitudes in both modes of reflection and transmission. The glucose concentration changes were reflected more prominently as amplitude variations in the resonance peaks of the harmonic resonances established towards higher frequencies 4.8–5.8 GHz (reflection response in Fig. 16(c)) and 3.5–5.1 GHz (transmission response in Fig. 16(d)), thus demonstrating the sensor capability to detect the small variations in the loss properties of the tested glucose samples. For repeatability verification, each glucose sample measurement was repeated for three times while paying attention to restore the exact reference response of the empty channel-loaded sensor after any sample removal as shown in Fig. 16(a) and 16(b). Each scattering plot is an average of three repeatable measurements for the respective glucose sample.

To verify the detection functionality of the sensor, it was experimented again for Hemoglobin samples of similar glucose concentrations 80, 100, 120 mg/dL using the setup in Fig. 17(a). The corresponding transmission responses were recorded in the higher frequency band 3.8–5.2 GHz where two distinct harmonic resonances were exhibited (Fig. 17(b) and 17(c)). It was observed that the first resonant frequency is reducing with an increased glucose level. However, the second resonance is not substantially affected by the change in glucose concentrations but rather changes its depth accordingly.

To avoid significant impact of any environmental and instrumental intakes onto the measurements, the sensing experiments were performed in an environment of controlled temperature 25 ± 1 °C mimicking indoor environments where such experiments are performed. However, small fluctuations in temperature will not significantly change the resonant amplitude readings of such CSRR structures (±0.03–0.09 dB/°C) [38]. Additionally, the tested glucose samples were all stored in the same room temperature of 25 ± 1 °C. This is necessary since the sensor scattering responses are enormously dependent on the glucose sample permittivity that is shown to be temperature dependent [38].

Authorized licensed use limited to: Universitat de Barcelona. Downloaded on October 17,2024 at 13:45:49 UTC from IEEE Xplore. Restrictions apply.

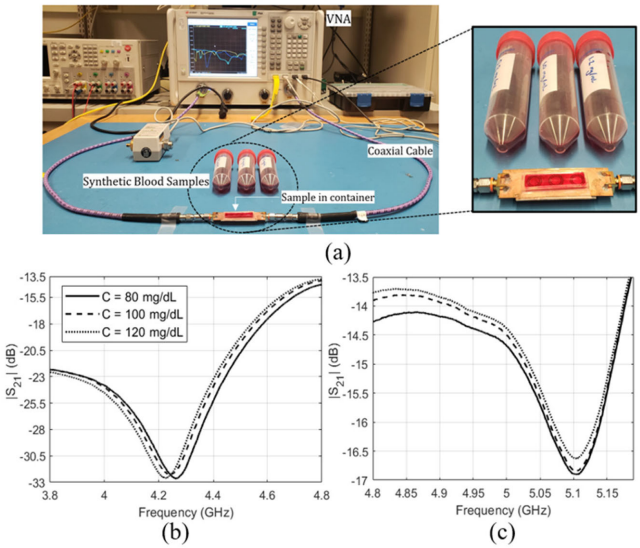

Fig. 17. Measurements of glucose in synthetic blood samples, (a) experimental setup, (b) and (c) measured transmission coefficients for different glucose samples in higher frequency bands.

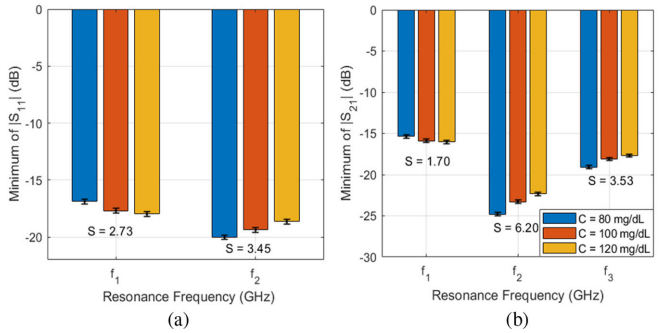

Fig. 18. Graphical illustration of the amplitude variations at each of the (a) reflection and (b) transmission resonances corresponding to glucose level changes. The sensitivity is shown for each resonance in dB/(mg/ml). Error bars are also attached to represent ±0.2 dB (reflection) and ±0.1 dB (transmission) variations in the three repeatable trials for each glucose sample.

B. Analysis of the Sensitivity and Repeatability Performance

The VNA experimental measurements of the S-parameters of the glucose-loaded TP-CSRR sensor have shown considerable variations in the peak amplitudes of the harmonic resonances of the S_{11} and S_{21} for varying the glucose levels between 80, 100, and 120 mg/dL. In what follows the sensitivity of the sensor is evaluated in terms of the absolute change in the magnitude of S_{21} or S_{11} (in dB) at any of the resonances corresponding to change in glucose concentration (in mg/ml). Two resonances $f_1 = 5.21$ GHz and $f_2 = 5.51$ GHz were recorded in the reflection response of the glucose-loaded sensor in the frequency range 4.8–6.0 GHz as indicated by the blue arrows in Fig. 16(c). It is observed that the reflected magnitude at f_1 slightly increases while that at f_2 decreases with increased glucose level. The average sensitivity at the two resonances was calculated as 2.73 and 3.45 dB/(mg/ml), respectively. Similarly, three distinct resonances $f_1 = 3.68$ GHz, $f_2 = 4.5$ GHz, and $f_3 = 4.92$ GHz (indicated by arrows in Fig. 16(d)) were recorded in the S_{21} transmission response of the sensor when used for glucose detection. The amplitude variations in the transmission resonances have shown to be more significant compared to their reflection counterparts as illustrated in Fig. 18. The harmonic resonance at $f_2 = 4.5$ GHz is the most sensitive mode where the glucose concentration of a tested sample can be distinctly detected with a considerable sensitivity of about 6.2 dB/(mg/ml) in average.

In the operating frequency range of the sensor, the data sheet of the VNA measuring tool used in these experiments poses for higher uncertainties in the readings of the reflection coefficient $|S_{11}|$ compared to the transmission coefficient ($\approx \pm 0.1$ dB uncertainty at -20–-25 dB transmission). This is also evidenced by the repeatability measurements that show ±0.2 dB variations in the resonant amplitudes of $|S_{11}|$ and ±0.1 dB for those in $|S_{21}|$. Therefore, magnitudes of resonance peaks in $|S_{21}|$ were adopted as more robust and reliable sensing parameters for the reported glucose measurements. By noting the resonant amplitudes recorded at the favorable $|S_{21}|$ resonance mode ($f_2 = 4.5$ GHz) of about -24.81 dB, -23.28 dB, and -22.33 dB amplitudes for the glucose concentrations 80, 100, and 120 mg/dL, respectively, thus yields a minimum resolution $\Delta|S_{21}|/\Delta|C|$ of about 0.05 dB/(mg/dL). Considering the ±0.1 dB uncertainty in VNA readings, this would imply that concentration changes as small as $\Delta C_{min} = 3$ mg/dL could be reasonably detected in the S_{21} signal using the proposed sensor when connected to the VNA. Therefore, larger glucose variations ($>= \Delta C_{min}$) would be reliably identifiable in the current setup since their corresponding amplitude changes are beyond the VNA noise limitation.

TABLE VII
COMPARISON BETWEEN STATE-OF-THE-ART MICROWAVE SENSORS USED FOR GLUCOSE DETECTION

Ref	Sample volume (μL)	Concentration (mg/ml)	Operating frequency (GHz)	Sensing parameter	S (dB per mg/ml)
[39]	7500	0.78 – 50	1.4 – 1.9	$\|S_{11}\|$	0.18
[38]	-	0 – 4	2.4 – 2.9	$\|S_{21}\|$	0.0075
[40]	-	0.3 – 80	7.5	$\|S_{21}\|$	0.008
[41]	170	5 – 25	1.91	$\|S_{21}\|$	0.025
[42]	20	200 – 1000	3.02	$\|S_{21}\|$	0.007
[43]	20	40 – 200	2.5 – 6	$\|S_{21}\|$	0.01
[44]	1000	0 – 300	2.0 – 2.5	$\|S_{11}\|$	0.003
This work	100 – 600	0.7 – 1.2	2.3 (unloaded) 1 – 6 (loaded)	$\|S_{11}\|/\|S_{21}\|$	1.7 – 6.2 (S_{21}) 0.6 – 3.45 (S_{11})

Lastly, in what follows the sensitivity of the proposed TP-CSRR sensor for glucose detection is compared to other microwave glucose sensors in the recent literature that adopted the resonant amplitude as a sensing parameter. Table VII presents a comparative summary of the state-of-the-art glucose sensors with their respective parameters: sample volume, tested concentrations, operating frequency, sensing parameter, and sensitivity in (dB/[mg/ml]). Careful examination of Table VII clearly demonstrates that the proposed TP-CSRR sensor outperforms other techniques and mechanisms in the literature for microwave sensing. In particular, the developed TP-CSRR has the capability to conveniently detect, within the range of normal glycemia, small variations of the glucose concentration with relatively high sensitivity. This major attribute along with the advantages of being non-destructive, low-cost, and simply fabricated in an electrically small size, lay the foundation for realizing a portable or wearable device for non-invasively monitoring blood glucose

Authorized licensed use limited to: Universitat de Barcelona. Downloaded on October 17,2024 at 13:45:49 UTC from IEEE Xplore. Restrictions apply.

levels in diabetics, including detection of hyperglycemia and hypoglycemia conditions. The sensor could also be used as a warning tool to diabetic patients when attempting to consume energy drinks and fruit juices which have inherently high glucose concentrations.

V. Conclusion

This paper developed and measured a novel microwave biomedical sensor operating in the cm-band of 1–6 GHz proposed for monitoring the glucose concentrations in the range of Type-2 diabetes. The sensing structure was efficiently designed using three circular-shaped complementary split ring resonators (CSRRs) in a thin sheet of a dielectric PCB. The CSRR sensing elements are coupled to a planar microstrip-line in the same structure thus allowing a compact portable model for real-time glucose level monitoring. The sensor capability for glucose detection was demonstrated by testing the glucose samples inside a vein-resembling rectangular channel integrated on top of the CSRRs surface where the electric field is highly intensified. The substantial interaction of the loaded glucose samples with the induced electric field perturbs the effective capacitance and resistance of the coupled CSRRs, thereby resulting into traceable variations in the reflection and transmission resonance peaks of high sensitivity to mutations in the complex permittivity of various concentrations. The desired performance of the fabricated sensor was practically validated through in-lab measurements for detecting the glucose in blood mimicking solutions of concentrations in the range 70–120 mg/dL for Type-2 normal diabetes. The sensor has shown to be highly sensitive to glucose level changes with a sensitivity performance of about 6.2 dB/(mg/ml) in $|S_{21}|$ which is superior to other existing sensors in terms of the resonance amplitude resolution. The proposed microwave sensor can be simply fabricated with low cost and miniaturized size, thus offering a great potential for integration with other microwave components in embedded sensors and systems-on-chip to realize a preliminary wearable or portable non-invasive device for glycemia level monitoring in real-time.

Future work on this research will consider the integration of multiple microfluidic channels with thin layers over the sensing region to mimic the actual scattering of blood inside capillaries, veins, and arteries vessels. A wearable prototype would also be realized on a flexible substrate of smaller dielectric constant and loss tangent to enhance its sensitivity when used for monitoring BGL directly from the subjects' fingers. Using a low-cost driving power source instead of the bulky VNA would also facilitate the on-body glucose sensing. However, the scalability among different diabetic patients with dissimilar blood characteristics will remain a challenge, and hence the need for invasive personal calibration.

References

[1] D. Whiting *et al.*, "Diabetes atlas: Global estimates of the prevalence of diabetes for 2011 and 2030," *Diabetes Res. Clin. Pract.*, vol. 94, no. 3, pp. 311–321, 2011.

[2] WHO, "WHO_World health day 2016_WHO calls for global action to halt rise in and improve care for people with diabetes," World Health Org., Geneva, Switzerland, Tech. Rep., 2016.

[3] American Diabetes Association, "Diagnosis and classification of diabetes-mellitus," *Diabetes Care*, vol. 37, pp. S81–S90, 2014.

[4] R. Holt, C. Cockram, A. Flyvbjerg, and B. Goldstein, *Textbook of Diabetes*. New York, NY, USA: John Wiley Sons, 2011.

[5] D. Cunningham and J. Stenken, *In Vivo Glucose Sensing*, Hoboken, NJ, USA: Wiley, 2010.

[6] W. V. Gonzales, A. T. Mobashsher, and A. Abbosh, "The progress of glucose Monitoring—A review of invasive to minimally and non-invasive techniques, devices and sensors," *Sensors*, vol. 19, no. 4, pp. 800–845, 2019.

[7] N. Spegazzini *et al.*, "Spectroscopic approach for dynamic bioanalyte tracking with minimal concentration information," *Sci. Rep.*, vol. 4, no. 7013, 2015.

[8] J. Y. Sim *et al.*, "In vivo microscopic photoacoustic spectroscopy for non-invasive glucose monitoring invulnerable to skin secretion products," *Sci. Rep.*, vol. 8, no. 1059, 2018.

[9] A. Hina and W. Saadeh, "A noninvasive glucose monitoring SoC based on single wavelength photoplethysmography," *IEEE Trans. Biomed. Circuits Syst.*, vol. 14, no. 3, pp. 504–515, Jun. 2020.

[10] E. V. Karpova *et al.*, "Noninvasive diabetes monitoring through continuous analysis of sweat using flow-through glucose biosensor," *Anal. Chem.*, vol. 91, no. 6, pp. 3778–3783, 2019.

[11] T. Karacolak *et al.*, "Cole-Cole model for glucose-dependent dielectric properties of blood plasma for continuous glucose monitoring," *Microw. Opt. Technol. Lett.*, vol. 55, no. 5, pp. 1160–1164, May 2013.

[12] R. Dobson *et al.*, "Blood glucose monitoring using microwave cavity perturbation," *Electron. Lett.*, vol. 48, no. 15, pp. 905–906, 2012.

[13] S. Wiwatwithaya *et al.*, "Real-time monitoring glucose by used microwave antenna apply to biosensor," in *Proc. 4th Biomed. Eng. Int. Conf.*, 2012, pp. 135–137.

[14] M. Hofmann *et al.*, "A novel approach to non-invasive blood glucose measurement based on RF transmission," in *Proc. MeMeA IEEE Int. Symp. Med. Meas. Appl.*, 2011, pp. 39–42.

[15] M. Hofmann *et al.*, "Non-invasive glucose monitoring using open electromagnetic waveguides," in *Proc. 42nd Eur. Microw. Conf.*, 2012, pp. 546–549.

[16] A. E. Omer, R. Hughson, S. Safavi-Naeini, and G. Shaker, "Blood glucose level monitoring using an FMCW millimeter-wave radar sensor," *Remote Sens. J.*, vol. 12, no. 3, pp. 385–409, 2020.

[17] S. Saha *et al.*, "A glucose sensing system based on transmission measurements at millimetre waves using micro strip patch antennas," *Sci. Rep.*, vol. 7, no. 6855, pp. 2017.

[18] M. A. H. Ansari, A. K. Jha, and M. J. Akhtar, "Design and application of the CSRR-Based planar sensor for noninvasive measurement of complex permittivity," *IEEE Sensors J.*, vol. 15, no. 12, pp. 7181–7189, Dec. 2015.

[19] A. Raj *et al.*, "Metamaterial-inspired microwave sensor for measurement of complex permittivity of materials," *Microw. Opt. Technol. Lett.*, vol. 58, no. 11, pp. 2577–2581, Nov. 2016.

[20] A. Ebrahimi, J. Scott, and K. Ghorbani, "Differential sensors using microstrip lines loaded with two split-ring resonators," *IEEE Sensors J.*, vol. 18, no. 14, pp. 5786–5793, Jul. 2018.

[21] A. Ebrahimi, J. Scott, and K. Ghorbani, "Transmission lines terminated with LC resonators for differential permittivity sensing," *IEEE Microw. Wireless. Compon. Lett.*, vol. 28, no. 12, pp. 1149–1151, Dec. 2018.

[22] H. Choi *et al.*, "Design and in vitro interference test of microwave non-invasive blood glucose monitoring sensor," *IEEE Trans. Microw. Theory Techn.*, vol. vol.63, no. 10, pp. 3016–3025, Oct. 2015.

[23] M. Islam *et al.*, "Left-handed metamaterial-inspired unit cell for s-band glucose sensing application," *Sensors*, vol. 19, no. 1, pp. 169–181, 2019.

[24] A. Kandwal *et al.*, "Highly sensitive closed loop enclosed split ring biosensor with high field confinement for aqueous and blood-glucose measurements," *Sci. Rep.*, vol. 10, no. 4081, 2020.

[25] C. G. Juan *et al.*, "Concentration measurement of microliter-volume water–glucose solutions using *q* factor of microwave sensors," *IEEE Trans. Instrum. Meas.*, vol. 68, no. 7, pp. 2621–2634, Jul. 2019.

[26] T. Yilmaz *et al.*, "Radio-frequency and microwave techniques for non-invasive measurement of blood glucose levels," *Diagnostics*, vol. 9, no. 1, pp. 6–39, 2019.

[27] S. Gabriel *et al.*, "The dielectric prperties of biological tissues: III. Parametric models for the dielectric spectrum of tissues," *Phys. Med. Biol.*, vol. 41, no. 11, pp. 2271–2293, 1996.

[28] C. Lee and C. Yang, "Complementary split-ring resonators for measuring dielectric constants and loss tangents," *IEEE Microw. Wirel. Compon. Lett.*, vol. 24, no. 8, pp. 563–565, Aug. 2014.

[29] A. E. Omer *et al.*, "Low-cost portable microwave sensor for non-invasive monitoring of blood glucose level: Novel design utilizing a four-cell CSRR hexagonal configuration," *Sci. Rep.*, vol. 10, 2020, Art. no. 15200.

Authorized licensed use limited to: Universitat de Barcelona. Downloaded on October 17,2024 at 13:45:49 UTC from IEEE Xplore. Restrictions apply.

[30] J. D. Baena *et al.*, "Equivalent-circuit models for split-ring resonators and complementary split-ring resonators coupled to planar transmission lines," *IEEE Trans. Microw. Theory Techn.*, vol. 53, no. 4, pp. 1451–1461, Apr. 2005.
[31] F. Deshours *et al.*, "Modeling of split ring resonators for the measurement of complex permittivities," XXIèmes Journées Nationales Microondes (JNM 2019), Caen, May 2019.
[32] M. Hofmann *et al.*, "Microwave-Based noninvasive concentration measurements for biomedical applications," *IEEE Trans. Microw. Theory Techn.*, vol. 61, no. 5, pp. 2195–2204, May 2013.
[33] A. E. Omer, S. Gigoyan, G. Shaker, and S. Safavi-Naeini, "WGM-based sensing of characterized glucose- aqueous solutions at mm-Waves," *IEEE Access*, vol. 8, pp. 38809–38825, 2020.
[34] A. E. Omer, G. Shaker, and S. Safavi-Naeini, "Portable radar-driven microwave sensor for intermittent glucose levels monitoring," *IEEE Sensors Lett.*, vol. 4, no. 5, pp. 1–4, May 2020.
[35] A. Brady, C. McCabe, and M. McCann, *Fundamentals of Medicalsurgical Nursing*. Hoboken, NJ, USA: John Wiley Sons, 2013.
[36] E. Topsakal, T. Karacolak, and E. C. Moreland, "Glucose-dependent dielectric properties of blood plasma," in *Proc. 30th URSI Gen. Assem. Sci. Symp.*, Istanbul, 2011, pp. 1–4.
[37] Scientific American. "Fake blood made scientific," Oct. 2015. Accessed: Sep. 2, 2020. [Online]. Available https://www.scientificamerican.com/article/fake-blood-made-scientific
[38] C. Jang *et al.*, "Non-Invasive fluidic glucose detection based on dual microwave complementary split ring resonators with a switching circuit for environmental effect elimination," *IEEE Sensors J.*, vol. 20, no. 15, pp. 8520–8527, Aug. 2020.
[39] S. Y. Huang *et al.*, "Microstrip line-based glucose sensor for noninvasive continuous monitoring using the main field for sensing and multivariable crosschecking," *IEEE Sensors J.*, vol. 19, no. 2, pp. 535–547, Jan. 15 2019.
[40] T. Chretiennot, D. Dubuc, and K. Grenier, "Microwave-based microfluidic sensor for non-destructive and quantitative glucose monitoring in aqueous solution," *Sensors*, vol. 16, no. 10, pp. 2016.
[41] G. Gennarelli *et al.*, "A microwave resonant sensor for concentration measurements of liquid solutions," *IEEE Sensors J.*, vol. 13, no. 5, pp. 1857–1864, May 2013.
[42] S. Harnsoongnoen and A. Wanthong, "Coplanar waveguides loaded with a split ring resonator-based microwave sensor for aqueous sucrose solutions," *Meas. Sci. Technol.*, vol. 27, no. 1, 2016, Art. no. 015103.
[43] S. Harnsoongnoen and A. Wanthong, "Coplanar waveguide transmission line loaded with electric-LC resonator for determination of glucose concentration sensing," *IEEE Sensors J.*, vol. 17, no. 6, pp. 1635–1640, Mar. 2017.
[44] S. Kim *et al.*, "Noncontact characterization of glucose by a waveguide microwave probe," *Curr. Appl. Phys.*, vol. 9, pp. 856–860, 2009.

Ala Eldin Omer (Student Member, IEEE) received his primary and secondary education in Khartoum, Sudan. He received the B.Sc. degree (magna cum laude) in electrical and electronics engineering with specialization in communication engineering from the University of Khartoum, Sudan, in 2013, and the M.Sc. degree (summa cum laude) in electrical engineering from the American University of Sharjah (AUS), in 2016, where he was awarded a two-year Graduate Assistantship from the Department of Electrical Engineering. He is currently working toward the Ph.D. degree with the Centre for Intelligent Antenna and Radio Systems (CIARS), Electrical and Computer Engineering Department, University of Waterloo, Canada. During his Ph.D., he has been working as a Visiting Research Assistant with the Group of Electrical Engineering of Paris (GeePs), Sorbonne University. From 2013 to 2014, he was a Research and Development Communication Engineer with the Telecommunication Research Centre (TRC), Khartoum, Sudan. In addition, since 2014, he has been with the Department of Electrical Engineering, AUS as a Teaching and Research Assistant. He has coauthored a number of journals, conference papers, and has been awarded many prestigious awards, Singapore International Pre-Graduate Award (SIPGA), IEEE-APS Doctoral Research Grant, NSERC CREATE fellowship, Erasmus+ mobility grant, and University of Waterloo Faculty of Engineering (FOE) awards. His research interests include communication systems, cognitive radio networks, micro/mm-wave sensing, bio-electromagnetics, complex wave propagation, radar systems, signal processing, and pattern classification.

George Shaker (Senior Member, IEEE) received the B.A.Sc., M.A.Sc., and the Ph.D. degrees. He is an Adjunct Professor with the Department of Electrical and Computer Engineering, University of Waterloo, where he is the Director of the Wireless Sensors and Devices Lab. He is a Research Lead with the Schlegel UW Research Institute for Aging. He is also with Spark Tech Labs, where he has been the Principal Scientist and the Head of Electromagnetics Research and Development, since 2011. Previously, he was with RIM's (Blackberry's) RF Research and Development Division. He was also with the Georgia Institute of Technology. Over the last two decades, he has led/contributed to launching more than 50 different wireless products to the market from startups and multinationals, with millions in sales to-date. Not including his technical reports, he has coauthored over 100 journal publications and conference papers, along with more than 30 patents/patent applications. He has received over 35 best paper awards and international recognitions.

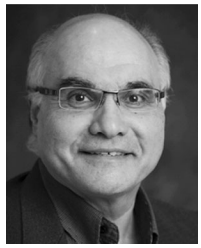

Safieddin Safavi-Naeini (Life Fellow, IEEE) received the B.Sc. degree from the University of Tehran, Tehran, Iran, in 1974, and the M.Sc. and Ph.D. degrees from the University of Illinois, Urbana–Champaign, Champaign, IL, USA, in 1975 and 1979, respectively, all in electrical engineering. He is currently a Professor with the Department of Electrical and Computer Engineering, University of Waterloo, Waterloo, Canada, and holds the Natural Science and Engineering Research Council (NSERC)/C-COM Satellite Systems Industrial Research Chair in Intelligent Radio/Antenna and Novel Electromagnetic Media, where he is also the Director of the Centre for Intelligent Antenna and Radio Systems (CIARS). He has coauthored more than 190 journal papers and 400 conference papers in international conferences. His current research interests include RF/Microwave technologies, smart integrated antennas and radio systems, mmW/terahertz integrated technologies, vehicular communication systems, emerging radio technologies for intelligent transportation systems (ITSs), nano-EM and photonics, EM in health science and pharmaceutical engineering, wireless communications and sensor systems and networks, new EM materials, bio-electromagnetics, biomedical instruments, and computational methods.

Georges Alquié received the high-level Doctorate from University Pierre and Marie Curie (UPMC and currently Sorbonne University) in 1977. He has been a Professor in Electrical Engineering since 1981. He is performing his research activities with the Group of Electrical Engineering of Paris (GeePs). He has been involved in the solid-state physics, microwave techniques, MMIC modelling and microwave photonics devices for telecommunications. He is the coninventor of three patents and was the Laboratory Manager and Initiator of several research collaborative projects. He is currently an Emeritus Professor with Sorbonne University and his research interest is mainly devoted to the field of microwave sensors for biological applications.

Authorized licensed use limited to: Universitat de Barcelona. Downloaded on October 17,2024 at 13:45:49 UTC from IEEE Xplore. Restrictions apply.

Frédérique Deshours Frederique received the Ph.D. degree in electronics and telecommunications from both Pierre and Marie Curie University (UPMC, France) and Telecom ParisTech (France) in 1996 She is currently an Associate Professor in electronics engineering with Sorbonne University (SU), mainly involved in the microwave techniques and electromagnetism. Her research interests include microwave and optoelectronic domains is performed with the Group of Electrical Engineering of Paris (GeePs). Her research interest has been extended to biomedical applications with the functional exploration of biological tissues. She is mainly involved in the design of microwave sensors for glucose level monitoring and atheromatous carotid lesions detection.

Hamid Kokabi (Member, IEEE) received the Dipl. Ing. degree in electrical engineering from ENSI-CAEN, France in 1989, and the M.Sc. and the Ph.D. degrees in material sciences for electronics from Caen University in 1990 and 1993 respectively. After he spent one year (1993/1994) in Japan as a Postdoc working on piezoelectric thin films for embedded strain sensors. He was with University Pierre and Marie Curie (UPMC currently Sorbonne University), Paris as an Assistant from 1994to 1996 and then Associate Professor from 1996 to 2005 and obtained his "Habilitation to lead research" in 2003 and Full Professor in 2005. He is the member of the Research Laboratory "Group of Electrical Engineering of Paris (GeePs)". His research interests include sensors and instrumentation and included passive electronic components and integrated piezoelectric sensors, microwave superconductivity, NDE using high Tc RF SQUIDs and other magnetic sensors for nonmagnetic metals. He has been in charge of the research theme on biomedical applications of electronics and electromagnetism since 2010. He is currently involved in research projects on sensors and systems for medical and biological applications including microwave miniaturized biosensors for glucose level sensing.

Raed M. Shubair (Senior Member, IEEE) received the B.Sc. degree (with Distinction and First Class Hons.) in electrical engineering from Kuwait University, Kuwait, in June 1989, and the Ph.D. degree (with Distinction) in electrical engineering from the University of Waterloo, Canada, in February 1993, for which he received the Distinguished Doctorate Dissertation Award. He is a Full Professor of Electrical Engineering affiliated with New York University (NYU) Abu Dhabi and with Massachusetts Institute of Technology (MIT). He has been a Full Professor of Electrical Engineering with Khalifa University (formerly, Etisalat University College), UAE, which he joined in 1993 up to 2017 during which he received several times the Excellence in Teaching Award and Distinguished service Award. He has authored or coauthored more than 350+ peer-reviewed journal and conference publications in several research areas including terahertz and wireless communications, modern antennas and applied electromagnetics, signal and array processing, machine learning, nano-biosensing and biomedicine. He is the Regional Director for IEEE Signal Processing Society in Middle East, Fellow of MIT Electromagnetics Academy, Founding Chair of the IEEE-UAE Innovations and Research Program, and Founding Chair of IEEE Chapter of New York University (NYU) Abu Dhabi. He has been a Nominee for the IEEE Distinguished Educator Award of IEEE Antennas and Propagation Society and is currently an invited speaker with the U.S. National Academies of Sciences, Engineering, and Medicine.

Authorized licensed use limited to: Universitat de Barcelona. Downloaded on October 17,2024 at 13:45:49 UTC from IEEE Xplore. Restrictions apply.